The Cryosphere
Discussions

Initialization of a global glacier model based on present-day glacier geometry and past climate information: an ensemble approach

Julia Eis[1], Fabien Maussion[2], and Ben Marzeion[1,3]

[1]Institute of Geography, University of Bremen, Bremen, Germany
[2]Department of Atmospheric and Cryospheric Sciences, University of Innsbruck, Innsbruck, Austria
[3]MARUM - Center for Marine Environmental Sciences, University of Bremen, Bremen, Germany

Correspondence: J. Eis (jeis@uni-bremen.de)

Abstract. To provide estimates of past glacier mass changes over the course of the 20th century, an adequate initial state is required. However, empirical evidence about past glacier states at regional or global scale is largely incomplete, both spatially and temporally, calling for the use of automated numerical methods. This study presents a new way to initialize the Open Global Glacier Model from past climate information and present-day glacier states. We generate a large set of physically plausible

5   glacier candidates for a given year in the past (e.g. 1850 in the Alps). All these candidates are modelled forward to the date of the observed glacier outline, and evaluated by comparing the results of the forward runs to the present-day states. We apply the approach on 2621 alpine glaciers and determine error estimates of the method from synthetic experiments. The results show that the solution is often non-unique, as many of the reconstructed initial states converge towards the observed state in the year of observation. We find that the median state of the best 5 percent of all acceptable states is a reasonable best estimate. The

10 accuracy of the method depends on the type of the considered observation for the evaluation (glacier length, area, or geometry). Trying to find past states from only present-day length instead of the full geometry leads to a sharp increase in uncertainty. Our method thus also provides quantitative information on how well the reconstructed initial glacier states are constrained through the combination of present-day outlines with past climate conditions. We show that even with perfectly known but incomplete boundary conditions the problem of model initialization is non-trivial and non-unique, and discuss ways to develop the method

15 further.

1   Introduction

Glaciers contributed significantly to past sea-level rise (SLR; e.g. Gregory et al., 2013; Slangen et al., 2017a; Cazenave and et al., 2018) and they will continue to be a major contributor in the 21th century (e.g. Church et al., 2013; Slangen et al., 2017b).

20 A large fraction of this contribution will be caused by the ongoing adjustment to the past climate (Marzeion et al., 2014, 2018). Reconstructions of past glacier mass change are therefore not only necessary to determine the budget of past sea-level change (Gregory et al., 2013) and to increase the confidence in projections (by allowing to quantify the agreement with observations,

Marzeion et al., 2015), they also enable us to quantify the pattern of the ongoing adjustment of glaciers to present-day climate. Estimates of global glacier mass change are based on in-situ measurements in mass and length changes (e.g. Zemp et al., 2015; Leclercq et al., 2011), on remote sensing techniques (e.g. Gardner et al., 2013; Jacob et al., 2012; Bamber et al., 2018), or on mass balance modelling driven by climate observations (Marzeion et al., 2012, 2015). Since observations of temperature,

5   and to a smaller degree, precipitation, are more ubiquitous (e.g. Harris et al., 2014) than glacier observations (WGMS, 2018), reconstructions of glacier change produced by forcing a glacier model with climate observations have the potential to increase the understanding of past glacier behaviour. Finally, reconstructing glacier change based on climate model output allows to test the skill of climate models (Goosse et al., 2018).

A number of global glacier models were developed in the past (e.g., Radić and Hock, 2011, 2014; Giesen and Oerlemans,

10 2012, 2013; Marzeion et al., 2012, 2014; Huss and Hock, 2015; Maussion et al., 2019). The more recent and complex of these models (e.g. Huss and Hock, 2015; Maussion et al., 2019) require Digital Elevation Models (DEMs) and outlines from the Randolph Glacier Inventory (RGI; RGI Consortium, 2017) to derive the initial surface hypsometry. The starting date of a glacier evolution simulation thus depends on the recording date of the DEM and the outline, which typically do not coincide with one another, nor with the required starting date of a projection. The model of Huss and Hock (2015) indicates a high

15 sensitivity to the initial ice volume. Similarly, Maussion et al. (2019) remark that great uncertainties, especially on local and regional scales, derive from unknown initial conditions.

Despite of the importance of glacier contribution to past sea-level rise, so far only one model was able to provide estimates of glacier mass changes over the course of the entire 20th century on the global scale (Marzeion et al., 2012). All other global modelling studies limit their application to the recent past and future projections. The reconstruction by Marzeion et al. (2012)

20 was possible because of the highly parameterized representation of ice dynamics and glacier geometry change, applying a Volume-Area-Time scaling to translate mass change into surface area and elevation range changes. Based on this approach, it was sufficient to iteratively optimize one variable (glacier size in the year of interest, e.g., 1850) such that when run forward to the year of the observed glacier outline, the modelled glacier area agreed with the observed glacier area.

An increase of model complexity impedes the process as more and more variables are required for initialization. Flowline

25 models require input data along the coordinates of the flowline (e.g. bed topography, surface elevations and/or widths) and thus more complex initialization methods are needed. For example, van Pelt et al. (2013) developed an iterative inverse method to reconstruct distributed bedrock topography and simultaneously initialize an ice flow model. Zekollari et al. (2019) added an ice flow model to Huss and Hock (2015) which required an automated initialization for glaciers in 1990 (prior to the glacier inventory date) to avoid spin-up issues and so that the reconstructed initial states fit the glacier geometry at the inventory date

30 after being modelled forward. By choosing a decade long initialization, they avoid problems of non-uniqueness (as we discuss below), but raise the question of how arbitrarily this date can be chosen. Similar approaches exists for the initialization of ice sheet models, where most work focuses on estimating the present-day state of ice sheets (e.g. Heimbach and Bugnion, 2009; Lee et al., 2015; Mosbeux et al., 2016). Goelzer et al. (2018) divide the existing initialization approaches into 3 methods: spin-up, assimilation of velocity, and assimilation of surface elevation. Spin-up procedures are typically used for long-term

35 and palaeoclimate simulations, the required spin-up time is unknown, can be relative long, and the reconstruction cannot be

expected to represent effects from internal climate variability correctly. The data assimilation approaches typically determine model parameters (e.g. basal parameters like basal friction or bedrock topography) that reduce the mismatch between observed and modelled velocities or surface elevations.

In this study, we aim to bring elements of response to the following questions:

5
- to which degree does the past evolution of a glacier constrain its present day geometry?

- how much information does the present day glacier geometry contain about its past states?

- is it possible to reconstruct past glacier states from the partial information available to us?

To this aim, we present a new method estimating past glacier states and apply it to synthetic numerical experiments. After introducing the relevant features of the Open Global Glacier Model (OGGM; Maussion et al., 2019) in Sect. 2.1, we describe
10 the design of the experiments in Sect. 2.3. The synthetic framework serves to test the skill of our approach in a surrogate model world where everything is known, and allows to apply data denial experiments to address the questions listed above. The initialization method is presented in Sect. 2.4. The developed method consists of 3 steps: generation of plausible glacier states, identification of glacier state candidates, and their evaluation based on the misfit between the modelled and the observed surface elevation at the year of the observation. We applied our approach to 2621 alpine glaciers and present the results for
15 the reconstructed initial states in the year 1850 in Sect. 4.1. The influence of the considered type of observation (e.g. glacier length, area or geometry) is shown in Sect. 4.2. Finally, we summarize the results and discuss the method's limitations and its applicability to real-case studies, as well as needed and possible future developments in Sect. 6.

2 Methods

2.1 The Open Global Glacier Model

20 The Open Global Glacier Model (OGGM; Maussion et al., 2019) is an open source numerical framework that allows the modelling of past and future changes of any glacier in the world. Starting with a glacier outline, provided by the Randolph Glacier Inventory (RGIv6.0; Pfeffer et al., 2014), a suitable surface DEM is automatically downloaded and interpolated to a local grid. The size of the local grid is given by a border parameter, which is the number of grid points outside the glacier boundaries. We choose a border value of 200 grid points to ensure that also large glacier states can be generated. The resolution
25 of the map topography dx depends on the size of the glacier and is constrained to $10\,m \leq dx \leq 200\,m$. After the preprocessing, glacier centerlines are computed using a geometrical routing algorithm (adapted from Kienholz et al., 2014). They are then considered as glacier flowlines, and grid points are generated using a fixed, equidistant grid spacing, which is twice that of the underlying 2D map topography. Surface elevations along the flowline coordinates are then obtained from the underlying topography file and glacier section widths are computed by intersecting the flowline's normal to the boundaries of the glacier.
30 By making assumptions about the shape of the bed (parabolic, rectangular or a mix of both), OGGM estimates the ice thickness with a mass-conservation approach (Farinotti et al., 2009, 2017, 2019). Information on bed topography at each grid point results

from the calculated ice thickness and the surface elevation. From this, the glacier's length, area, and volume can be determined. These values depend strongly on the surface topography and are based on the (often wrong) assumption that the recording date of DEM and that of the outline coincide. The model then computes the glacier mass balance at each grid point using climate data (monthly temperature and precipitation). Climate data can be used from different sources, including gridded observations or

5   reanalyses for past climate, projections for future climate, or randomized climate time series for more specialized applications. To force the mass balance model with a randomized climate time series, a window size h and a center year y_0 need to be set first. All years $\in [y_0 - \frac{h-1}{2}, y_0 + \frac{h-1}{2}]$ are then shuffled in the next step. Additionally, it is possible to set a temperature bias β, which shift all values of the temperature series. The objective of forcing the mass balance model with randomized climate is to easily produce a great number of realistic climate settings, representative of a given time period. The dynamical flowline

10 model can then be used to determine the evolution of the glacier under certain climate forcings by solving the shallow ice approximation.

For more details concerning the glacier model, please refer to Maussion et al. (2019) and http://docs.oggm.org.

2.2   Problem description

Here, we define a *glacier state* (hereinafter referred as *state*) as follows:

15 **Definition 1.** *Let* $m \in \mathbb{N}$ *be the total number of grid points of all flowlines of a glacier. Then* $s_t = (z_t, w_t, b)$ *is a* **glacier state** *at time t, with surface elevation* $z_t \in \mathbb{R}^m_+$, *widths* $w_t \in \mathbb{R}^m_+$, *and bed topography* $b \in \mathbb{R}^m_+$. *The set* $\mathcal{S}_{t_i} = \{s_t | t = t_i\}$ *contains all physically plausible glacier states at time* t_i.

The construction of an initial state is an inverse problem and can be defined in opposition to the direct problem.

The *direct problem* corresponds to a forward model run:

20

Given an initial state $s_{t_0} \in \mathcal{S}_{t_0}$ at time t_0, the state $s_t \in \mathcal{S}_t$ at time $t > t_0$ can be computed by:

$$s_t = G_{\text{past}}(s_{t_0}) \tag{1}$$

where $G_{\text{past}} : \mathcal{S}_{t_0} \to \mathcal{S}_t$ is an operator representing the equations of OGGM, using known climate time series as boundary condition.

25

For *inverse problems*, the solution is known by direct observations: $s_{t_e} = s^{obs}_{t_e}$, whereas the desired initial state s_{t_0} is unknown. The inverse problem consists of finding the initial state $s_{t_0} \in \mathcal{S}_{t_0}$, such that the forward modelled solution at time t_e fits the observations from the same year t_e:

$$s_{t_0} = G^{-1}_{\text{past}}(s^{obs}_{t_e}) \tag{2}$$

30 Unfortunately, we do not have an explicit formulation for G^{-1}_{past} in our case. A backwards reconstruction is impeded by the non-linear interaction between glacier geometry, ice flow and mass balance. Optimization methods can be used to solve inverse

problems. To this end, we introduce a minimization problem such that the forward modelled state is as close as possible to the observation:

$$\min_{s_{t_0} \in \mathcal{S}_{t_0}} j(s_{t_0}) \tag{3}$$

with

5 $$j(s_{t_0}) := \frac{1}{m} \parallel s_{t_e}^{obs} - \underbrace{G_{\text{past}}(s_{t_0})}_{s_{t_e}} \parallel_2^2 = \frac{1}{m} \left(\sum_{i=0}^{m} \left((z_{t_e}^{obs})_i - (z_{t_e})_i \right)^2 + \left((w_{t_e}^{obs})_i - (w_{t_e})_i \right)^2 + \underbrace{\left((b^{obs})_i - (b)_i \right)^2}_{=0} \right) \tag{4}$$

This function calculates the averaged difference in surface elevation and width between the observed and forward modelled glacier state. Differences in bed topography can be neglected, as we assume the bed topography to remain the same over the inspected time period.

In many cases, however, OGGM's forward integrations of different initial states result in very similar states at time t_e. This

10 implies that there exist many local minima of the function $j(s_{t_0})$. As uncertainties of the model can safely be assumed to be larger than the differences between those states at time t_e, it is impossible to identify the global minimum of $j(s_{t_0})$. I.e., the solution of our inverse problem is non-unique.

The objective of our approach is therefore to identify the set $\mathcal{S}_{t_0}^\epsilon$ of all states which correspond to the observed state $s_{t_e}^{obs}$ within a given uncertainty ϵ after being modelled forward. We call this condition *acceptance criterion*:

15 $$J(s_{t_0}) := \frac{j(s_{t_0})}{\epsilon} < 1 \tag{5}$$

The function $J(s_{t_0})$ is called in in the following *fitness function*. Assuming a vertical error of 5 m in x and an horizontal error of 10 m in w, we propose to set $\epsilon = (5\text{m})^2 + (10\text{m})^2 = 125\text{m}^2$. These numbers can be changed easily, and in a real-world application should be based on the vertical uncertainty of the used DEM and the horizontal uncertainty of the used outline. All states $s_{t_0} \in \mathcal{S}_{t_0}^{125}$ that have a fitness value smaller than one are called *acceptable states*. The first expectation would be that

20 the glacier with the smallest fitness value, is be the best solution. However, due to uncertainties that derive from the model itself, this is not always the case. As an alternative, we determine the 5th quantile of all states in $\mathcal{S}_{t_0}^\epsilon$. This set contains the best solutions of all acceptable states referred to the fitness value. We choose the median state, as a representative of this set and compare the state with the minimal fitness value and the median state in Sect 4.1.

2.3 Synthetic experiments

25 In order to be able to evaluate the results of the initialization method, we use synthetic experiments. To this end, we use OGGM to initialize a model run. We apply a random climate scenario (window size $h = 31$ years, and center year $y_0 = t_0$) and run the model 400 years forward. The temperature bias is set to $\beta = -1K$ to ensure that a relatively big glacier state is created, because this the case for most real glaciers in 1850. The resulting state is defined to be the state in year t_0. We model this state forward, applying the past climate time series from t_0 until t_e (here: 2000) and obtain the *observed* state of the synthetic experiment.

30 Through this procedure, a time series of glacier states is created, which in the following we will try to recover applying the

initialization method described below, but only using information about the observed state from the synthetic experiment in t_e. Thanks to the initial temperature bias of $\beta = -1K$, these synthetic states in t_e are close to the real observed states in 2000 (total area difference of about 1%, but individual glaciers can vary). In the following we call the state derived from the synthetic experiment s_t^{exp}.

Figure 1 shows the surface elevations in 1850 and 2000 of the synthetic experiment for the Guslarferner as an example.

Figure 1. Synthetic experiment applied to the Guslarferner (Alps). Cross-Sections along the main flowline in **a:** $t_0 = 1850$ and **b:** $t_e = 2000$. Black line indicates the bed rock and the dashed line the ice surface of the synthetic experiment.

We will discuss the limitations of the usage of the synthetic experiments in the context of real-world applications in Sect. 6.

2.4 Reconstruction of initial glacier states

Our initialization method consists of three main steps: generation of a set of physically plausible glacier states $\mathcal{S}_{t_0}$, identification of glacier candidates $s_{t_0} \in \mathcal{S}_{t_0}$, and their evaluation based on the fitness function $J(s_{t_0})$ (see Sec. 2.2).

2.4.1 Generation of glacier states

In a first step, we generate a set of different, physically plausible states. For this purpose, we utilize a random mass balance model with a window size of $h = 31$ years and the center year $y_0 = t_0$ to create different climate conditions. Obviously, we do not use the same permutation as for the creation of the synthetic experiments (see Sect. 2.3). This procedure has the advantage that a realistic climate representative of a given time period can be created, while interannual variability is uncorrelated to that of the period. Hence, all generated climate models differ from each other, but represent the climate conditions around t_0 at the same time. Additionally, we vary the temperature bias β to create further variations. We start with temperature biases
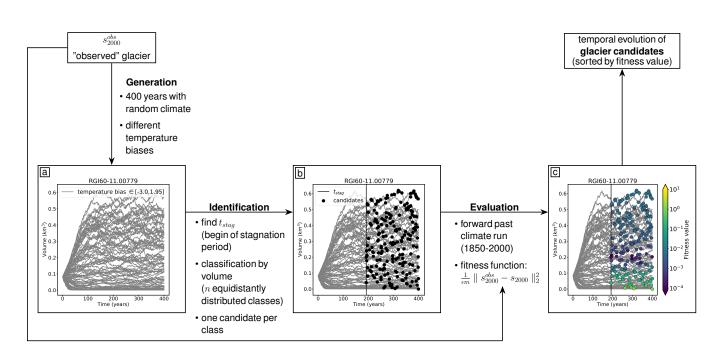
Figure 2. Workflow of the initialization method, using Guslarferner (Alps) as an example. **a:** The generation of different glacier candidates. The grey lines indicate the glacier volume evolution for a set of different random climate scenarios over 400 years each. The temperature biases vary between -2.65 and 2.95 K. **b:**The black vertical line indicates t_{stag} and the black points show 200 candidates. **c:** The glacier candidates colored by their fitness value. Violet marks candidates with a small missfit, whereas yellow marks states that don't meet the acceptance criterion (Eq. 5).

$\beta \in [-2,2]$ K. If $\beta = 2$ K is not large enough to result in a glacier with zero ice thickness, higher values will be used. If $\beta = -2$ K is not small enough to result in a glacier that reaches the boundary of the local grid (200 grid points outside of the glacier's boundary), smaller values will be used. We use these climate conditions to force a 400-year glacier simulation. 400 years turned out to be a sufficient time to generate a large number of different states. This model run is initialized with the only known state,
5 which is the actual observed glacier topography, taken from the RGI (see Fig. 2a).

2.4.2 Identification of candidates

Figure 2a shows the evolution of the volume of the generated glacier states over time. In the first years, the time series clearly diverge (mostly caused by the temperature bias β), but after a certain time all time series begin to fluctuate around an equilib-
10 rium value. We refer to the period of fluctuations around the assumed equilibrium as the *stagnation period*. We define t_{stag} as the point in time where all trajectories have reached this stagnation period. The required time to reach a stagnation period is longer for thicker glaciers (Jóhannesson et al., 1989). Glacier volume increases with decreasing temperature biases. Thus, we choose the upper ten volume trajectories, corresponding to the lowest temperature biases, to determine t_{stag}. To this end, we

smooth each of the ten curves and calculate the time point of their first maximum. t_{stag} is defined as the latest of all previously determined time points (see Fig. 2b).

Defining t_{stag} is necessary, because we determine initial glacier states at $t_0 = 1850$ and the searched glaciers are assumed to be in equilibrium with the climate around 1850. Hence, each state that fluctuate around an equilibrium value is a potential glacier

5 state candidate (in the following referred as candidate). This holds true for all states s_t with $t > t_{stag}$. In order to avoid testing very similar states, we classify all states by their volume and select one candidate per class. We choose n equidistantly and approximately uniform distributed classes, where n (default: $n = 200$) is the number of candidates to evaluate in step three.

2.4.3 Evaluation

The last step evaluates all previously selected candidates. Each candidate is used as initial condition for a forward run, using

10 observed past climate time series, e.g. from $t_0 = 1850$ until $t_e = 2000$. All runs use the same model parameter set, except for the initial condition and exactly the same climate time series. Afterwards, we compare the resulting modelled states s_{t_e} with the observed state $s_{t_e}^{obs}$ by applying the fitness function $J(s_{t_0})$ (Eq. 5). This function calculates the averaged difference between the glacier geometries at the grid points, more specifically between the surface elevations z_{t_e} and the widths w_{t_e}, of the observed and the modelled glacier. In Fig. 2c the candidates are colored by their fitness value. The resulting output of this

15 method is the temporal evolution of all candidates from t_0 until t_e sorted by their fitness value.

3   Test site and Input Data

We tested our approach on alpine glaciers. The glacier outlines are derived from the Randolph Glacier Inventory (RGI v6.0, region 11; Pfeffer et al., 2014). For each of the glacier outlines a transverse Mercator projection, which is centered on the glacier, is defined in order to preserve map projection properties (e.g. area, distances, angles). Next, the topographical data is

20 automatically downloaded by OGGM. The source of the DEM is the Shuttle Radar Topography Mission (SRTM) 90m Digital Elevation Database v4.1 (Jarvis et al., 2008) as the study area is located in the $[60°S; 60°N]$ range (Maussion et al., 2019) and the aquisition date (2000) matches well that of the RGI (2003). The climate dataset we use for this approach is the HISTALP database (Auer et al., 2007, http://www.zamg.ac.at/histalp). The temperature time series covers the period 1780 to 2014 and the precipitation time series 1801 to 2014. Both data sets are available on a regular grid of 5 minutes resolution.

25 We generate synthetic experiments (see Sect. 2.3) for all glaciers in the Alps, and determine their glacier states in 1850 if the area of the observed synthetic state s_{2000}^{exp} is larger than $0.01km^2$. This value is consistent with the minimum-area threshold of the RGI. The condition is satisfied for 2621 synthetic experiments of the 3927 glaciers included in the Randolph Glacier Inventory in Central Europe (region 11).

4 Results

Here we show (i) the results for two example glaciers in 1850, as well as an error analysis for all tested glaciers, and (ii) the influence of the choice of the fitness function on the quality of our results.

4.1 Initial glacier states in 1850

5   Following the method described in Sect. 2.4, we determine reconstructed initial glacier states in $t_0 = 1850$. Figures 3 and 4 show the results of the Guslarferner, as an example glacier. A second case, the Hintereisferner, is shown in Fig. 5 and 6. Especially the result of the Guslarferner shows clearly that the determination of past states is not unique (see Fig. 3). Multiple initial states (violet and blue colored) merge to the observed state in the year of observation. The fitness values, which means the averaged difference between the forward modelled states and the observation at $t_e = 2000$, are extremely small for most

10   candidates. The fitness values of all candidates range from 1.6×10^{-5} to 1.26. Only two of the 200 candidates has a fitness value higher than one and thus do not fulfill the acceptance criterion (Eq. 5); for these states, the glacier in 1850 is too small to reach the volume of the observed glacier within 150 years. Also Fig.4 illustrates the diversity of the different acceptable solutions (grey, shadowed area). The length of all states in S_{1850}^{125} varies between 0.5 km and 8.3 km. The acceptance criterion in this example is not strong enough to provide any information about the searched state in $t_0 = 1850$, as any of the candidates would lead to an acceptable result. Figure 4 also shows the 5th percentile of all acceptable states (blue, shadowed area). This

15   set contains the 5 % best solutions, based on the fitness value. All candidates of the 5th percentile are in close proximity to the synthetic experiment. The range of fitness values of all candidates of the 5th percentile is $[1.6 \times 10^{-5}, 1.84 \times 10^{-4}]$ and the length of the states in 1850 only varies from about 3 km to 4.1 km. All these candidates match the observation in $t_e = 2000$ very well and converge to the synthetic experiment by 1880 at the latest, which can be seen in Fig. 4c. As a representative of this set,

20   we choose the median state of the 5th percentile of S_t^{125} (in the following referred as s_t^{med}). Figure 4a shows that the surface elevation of s_{1850}^{med} in 1850 corresponds very well to the synthetic experiment, whereas the state with the minimum fitness value (in the following referred as s_t^{min}) slightly mismatches the synthetic experiment at the tail of the glacier. Regarding the volumes, neither s_t^{med} nor s_t^{min} match exactly the volume of the synthetic experiment in 1850, but the differences are small ($0.007\ km^3$ for s_t^{med} and $0.008\ km^3$ for s_t^{min}).

25   The results of Hintereisferner are different to the results from Guslarferner (see Fig. 5). The fitness values of most candidates are large compared to the ones of the Guslarferner. Only a few candidates have extremely small fitness values. In the case of the Hintereisferner, the past state is thus much more narrowly confined. The different states need more time to adapt to the climate conditions and therefore they do not converge as quickly to one state. As a result, the differences between the forward modelled states and the observed one in 2000 are larger. The fitness values of all candidates range between 1.2×10^{-3} and 47.

30   68 candidates fulfill the acceptance criterion (Eq. 5). Figure 6 shows that the acceptance criterion in this case confines the method better than in the case of the Guslarferner. The length of all glaciers in S_{1850}^{125} range from 8.5 km to 15.7 km. In this case the 5th quantile of S_t^{125} is again in close proximity to the synthetic experiment and all candidates of the 5th quantile have extremely small fitness values (between 1.2×10^{-4} and 2.16×10^{-3}). The length of the candidates of the 5th quantile in 1850 only
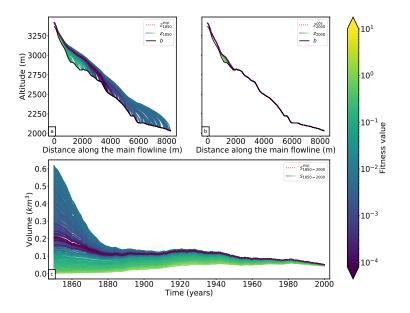
RGI60-11.00779: Guslarferner

Figure 3. Results for the Guslarferner. Top: Cross-sections along the main flowline in **a:** 1850 and **b:** 2000. Black line indicates the bed rock, the red, dotted line the surface elevation from the synthetic experiment, and the remaining lines the modelled ice surfaces of all candidates, colored by their fitness value. Bottom: Volume changes from 1850-2000, colored by their fitness values.

varies from 11.7 km to 12.4 km and is thus more precise than in the Guslarferner example. Also in this example, all candidates of the 5th percentile converge not later than 1880 to the state of the synthetic experiment. s_t^{med} matches the surface elevation of the synthetic experiment in 1850, as well as the volume trajectory over time, slightly better than s_t^{min}, but the volume differences to the synthetic experiments in 1850 are also very small in this example (0.007 km^3 for s_t^{med} and 0.03 km^3 for s_t^{min}).

For both examples we were able to show, that our method is able to determine the state in $t_0 = 1850$ of the synthetic experiment by only using information about the observed state of the synthetic experiment in $t_e = 2000$ and combining it with information about the past climate evolution. s_t^{med}, as well as s_t^{min} match the synthetic experiment in $t_0 = 1850$ extremely well. In the following, we provide an error analysis including all glaciers in the Alps to which we applied our method.

For each of the 2621 glaciers we have calculated the absolute volume error:

$$e_{abs}^{med/min}(t) = v^{med/min}(t) - v^{exp}(t), \tag{6}$$

where $v^{exp}(t)$ is the volume of the synthetic experiment in year t and $v^{med/min}(t)$ is the volume of s_t^{med} or s_t^{min} in the same year t. Figure 7 shows the absolute volume errors in km^3 for s_t^{med}, as well as for s_t^{min}. Whereas the absolute volume errors in 1850 vary widely from approx. -0.45 km^3 to 8 km^3, they reduce rapidly within 50 years. In 1900, the errors range from
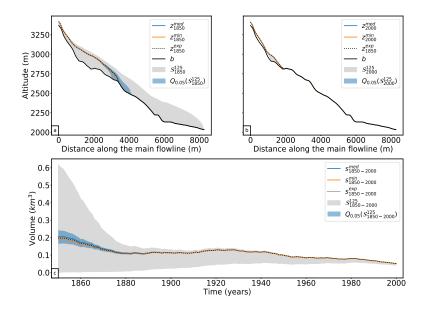
The Cryosphere
Discussions

Figure 4. Results for the Guslarferner. Top: Cross-sections along the main flowline in **a:** 1850 and **b:** 2000. Bottom: Volume changes from 1850-2000. The grey shaded area indicates the range of all solutions with a fitness value smaller than one ($\mathcal{S}_t^{125}$). The blue shaded area shows the range of the 5th quantile of $\mathcal{S}_t^{125}$, the blue line s_t^{med}, and the orange line s_t^{min}.

approx. $-0.17\ km^3$ to $0.3\ km^3$. The range of errors in the first 50 years is largely influenced by a few single outliers. Differences between s_t^{min} and s_t^{med} are small. Figure 8 shows the median and the range of the 5th-95th percentile of e_{abs}^{med} and e_{abs}^{min} over time, indicating the robustness of our method. The median of e_{abs} of both analyzed states is very small; $0.0033\ km^3$ for s_t^{min} and $0.0044\ km^3$ for s_t^{med} in 1850. The improvement with time can also be seen here: the median of $e_{abs}^{med}(1900)$ is of the order

5 of $10^{-5}\ km^3$ and that of $e_{abs}^{min}(1900)$ of the order of $10^{-6}\ km^3$. 2490 of the 2621 sates with a minimal fitness value s_t^{min} (95 % of the tested glaciers) have in 1850 an absolute volume error smaller than 0.1 km^3. Regarding s_t^{med}, 95 % of the glaciers even have in 1850 error values smaller than 0.08 km^3.

As our test site contains large and small sized glaciers, we also evaluate relative errors (in %):

$$e_{rel}^{med/min}(t) = \frac{e_{abs}^{med/min}(t)}{v^{exp}(t)} * 100 \tag{7}$$

10 Figure 9a shows the histogram of the relative errors in 1850, whereas the the evolution from 1850-2000 of the median and the 5th-95th percentile of the relative errors are shown in Fig. 9b. The median of the relative volume errors in 1850 is 14.8 % for s_t^{med} and 10.4 % for s_t^{min}. The 95th percentile value of e_{rel}^{min} is 286 %. With 248 % the value of e_{rel}^{med} is slightly smaller for the s_t^{med}.

Whereas s_t^{med} have in 1850 a slightly smaller 5th-95th percentile range than s_t^{min}, the median error of s_t^{min} is slightly smaller
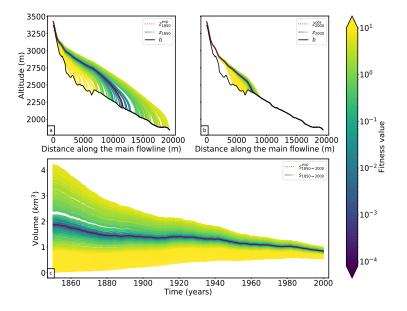
11

Figure 5. Results for the Hintereisferner. Top: Cross-sections along the main flowline in **a:** 1850 and **b:** 2000. Black line indicates the bed rock, the red dotted line the surface elevation from the synthetic experiment ,and the remaining lines the modelled ice surfaces of all candidates, colored by their fitness value. Bottom: Volume changes from 1850-2000, colored by their fitness values. All violet and blue glacier states merge to the observed glacier in 2000.

than the one of s_t^{med}.

Both states fit well the synthetic experiment. In many cases, s_t^{med} is equal to s_t^{min}, but for some glaciers either s_t^{min} or s_t^{med} have a clearly better performance. In all cases, the uncertainties quickly reduce after around 1880 to 1900. The error analysis also shows that our method has a slight tendency to overestimate the glacier volume, and that the error distribution is strongly
5 skewed (see Figure 9a).

4.2 Impact of the fitness function

For the evaluation of the glacier candidates we used a fitness function based on differences in the geometry of the glacier (see Eq. 5). In this section we want to test the influence of limited information on glacier geometry on the reconstructabilty of past glacier states. Thus, we additionally evaluate the candidates by only using information about the glacier area or length.
10 For the glacier area based evaluation, we used the following fitness function:

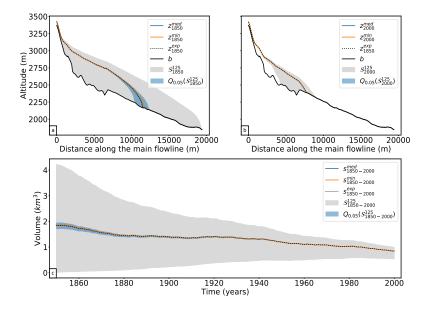$$J_A(A_{t_e}) = (A_{t_e}^{obs} - A_{t_e})^2 \tag{8}$$

The Cryosphere
Discussions

Open Access

EGU

Figure 6. Results for the Hintereisferner. Top: Cross-sections along the main flowline in **a:** 1850 and **b:** 2000. Bottom: Volume changes from 1850-2000. The grey shaded area indicates the range of all solutions with a fitness value smaller than one ($\mathcal{S}_{1850}^{125}$). The blue shaded area shows the range of the 5th quantile of $\mathcal{S}_t^{125}$, the blue line shows s_t^{med}, and the orange line s_t^{min}.

where A_{t_e} is the glacier area at time t_e. The fitness function that takes only information about the glacier length $l(t_e)$ at time t_e into account is similar:

$$J_l(l_{t_e}) = (l_{t_e}^{obs} - l_{t_e})^2 \tag{9}$$

For each glacier in our test site, we evaluate the 200 candidates also with the fitness functions J_A and J_l. For each evaluation
5   method (geometry, area and length based), we determine the state with the minimal fitness function [1] and calculate the relative volume error to the synthetic experiment.

     Figure 10 shows the relative errors of all three evaluation methods. Figure 9a shows the distribution of the relative errors of the 5th-95th percentile in 1850, whereas the the evolution from 1850-2000 of the median and the 5th-95th percentile of the relative errors are shown in Fig. 9b. The more information is taken into account for the evaluation, the smaller are the errors.
10   The greatest uncertainties are associated with using the glacier length based fitness function (Eq. 9), whereas the differences between the area based evaluation (Eq. 8) and the geometry based evaluation (Eq. 5) are small. While the median errors in 1850 of the geometry and the area based evaluation are close (10.4% for the geometry and 11.5 % for the area approach), the median

---

[1]Instead, it is also possible to choose s_t^{med} for the uncertainty analyses, but this would require acceptance criteria for the fitness functions J_A and J_l, which would have influence on the state. For simplification, we choose the state with the minimal fitness function.
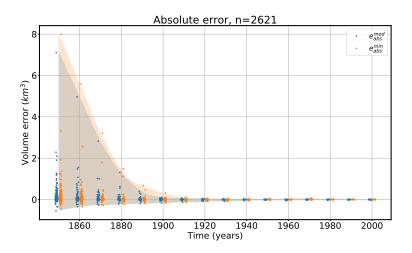
Figure 7. Absolute volume errors in km^3 over time of s_t^{min} and s_t^{med} of all tested glaciers. The blue points mark the individual errors e_{abs}^{med} of s_t^{med} and the orange points mark the individual errors e_{abs}^{min} of s_t^{min} . The blue, shadowed area shows the total range of the errors of the s_t^{med} and the orange, shadowed area the total range of errors s_t^{min} .
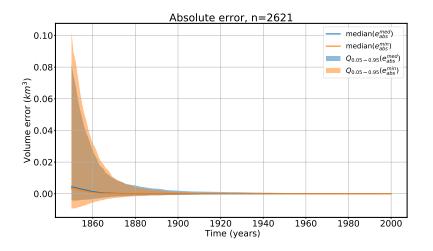

Figure 8. Median and the range between the 5th and 95th percentile ($Q_{0.05-0.95}$) of the absolute volume errors e_{abs}^{med} and e_{abs}^{min} over time.
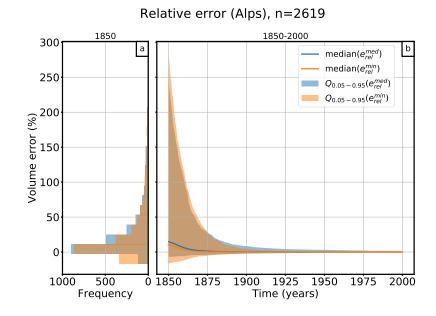
14

Figure 9. Relative volume errors of s_t^{med} (blue colored) and s_t^{min} (orange colored). Figure **a:** shows a histogram of all errors in the 5th-95th percentile in year 1850 and **b:** the evolution of the relative errors from 1850-2000. The line indicate the median error and the shadowed area the 5th-95th percentile range $Q_{0.05-0.95}$.

error in 1850 of the glacier length evaluation has with 137% the worst performance. This holds also true regarding the values of the 95th precentile; 95% of the tested cases have in 1850 a relative volume error smaller than 1008%, if the length based fitness function is used for the evaluation. For the area based evaluation this value is 329% and for the geometry based fitness function 95% of the tested glaciers have an error smaller than 286%. This shows that the advantage using the geometry instead

5 of the glacier area to evaluate the candidates is not very high; both evaluations shows a very good performance. Especially if the states are modelled forward (e.g. to 1900), both approaches perform well. However, it is not advisable to use the glacier length based evaluation.

5 Hardware requirements and performance

For this study we used a small cluster comprising two nodes with two 14-core CPUs each, resulting in 112 parallel threads

10 (two threads per core). Our method requires to run hundreds of dynamical model runs for each single glacier and as described in Maussion et al. (2019) the dynamical runs are the most expensive computations. The size of the glacier and the required time stepping to ensure a numerical stability influence strongly the required computation time. The computation time needed to apply our initialization procedure to one glacier varies from 30 seconds to 37 minutes. In total initializing the 2621 glaciers in 1850 took 3.5 days on our small cluster.
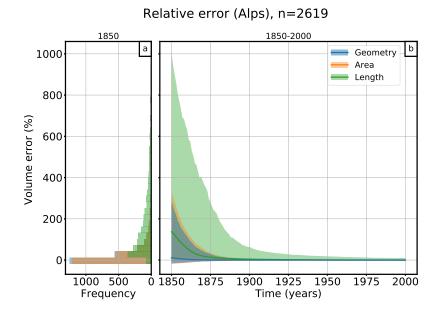
Figure 10. Relative volume errors of s_t^{min} derived from different fitness functions based on the geometry (blue), the glacier area (orange) and glacier length (green). Figure **a:** shows a histogram of all relative errors in the 5th-95th percentile in year 1850 and **b:** the evolution of the relative errors from 1850-2000. The line shows the median error and the shadowed area the 5th-95th percentile range.

6   Discussion and conclusions

In this study, a new method to initialize past glacier states is presented and applied in synthetic experiments. Assuming a perfectly known world allows us to identify the errors of our method alone and to separate them from uncertainties in obser-vations and errors introduced by model approximations. A differentiation between the different error sources in a real-world application is difficult and thus an evaluation of the skill of the method would be difficult, too. For real world applications, we will have to validate the reconstructions against past outlines derived from moraines, historical maps or remote sensing (e.g. as provided by GLIMS, Raup et al., 2007).

Similarly, our results do not provide information about actual past glacier mass change. Since in our synthetic experiments glaciers states in 2000 may be different from the real ones, the modelled initial glacier states in 1850 do not correspond to reality either. The past states determined in this study only can serve to verify the functionality of the developed method.

The results in Sect. 4.1 have shown that the solutions are not unique. Multiple candidates match the observation in $t_e = 2000$, sometimes with a large spread. This raises interesting questions about the use of past glacier change information to reconstruct climate variations, which we don't address here. In the context of model initialization, this non-uniqueness is impeding the re-construction. We evaluated the candidates with a fitness function based on averaged geometry differences between the forward modelled and the observed state in $t_e = 2000$. The threshold value $\epsilon = 125$ m^2 was derived by assuming a typical error of 5 m in surface elevations and 10 m in glacier width, but how these values should be chosen depends on the situation. Especially

in cases where many of the candidate states have extremely small fitness values, a more strict acceptance criterion can help to narrow the results. Otherwise, an ϵ that is too strict could lead to none of the candidates fulfilling the criterion.

Due to uncertainties that derive from the model itself, the glacier state with the minimal fitness value is not always close to the synthetic experiment. As a more robust alternative, we propose to use s_t^{med}, the median state of the 5th percentile of all

5 acceptable states as the best estimate. In Sect. 4.1 we compared the errors of both approaches. On the one hand, the median error of s_t^{min} is slightly smaller than that of s_t^{med}. On the other hand, the total range of errors is smaller for s_t^{med}. Modelling the reconstructed initial states forward in time approximately 50 years leads to a rapid reduction of the error, and s_t^{min} and s_t^{med} perform equally good.

In Sect. 4.2 we compare different fitness functions for the candidate evaluation. We show that using limited information only

10 (glacier area and glacier length) lead to an increase of the errors in 1850. The differences between the geometry based evaluation and the area based evaluation are small, but the differences to the length based evaluation are significant. This reflects that glacier states with the same length could differ strongly in volume and area. But this effect is also influenced by the spatial resolution of the model grid: a higher resolution of the grid would lead more variability in fitness values and hence to a more precise initialization. At the same time, a higher resolution would increase the computational demands of the initialization

15 method. We strongly recommend to use either the geometry or the area based fitness function for the evaluation. In this study, we only take the observation of the year t_e into account. Multi-temporal outlines would greatly reduce uncertainties at prior times.

Our results are relevant for future glacier evolution modeling studies, as they indicate that at least for some glaciers the time needed to converge to a similar evolution regardless of the 1850 state is comparatively short. A correlation analysis of the

20 estimated reconstruction spread and error with glacier characteristics (e.g. size, slope, ice thickness distribution per altitude, climatic setting, etc.) may lead to improved understanding of the factors that influence the reconstructability of a glacier's past states, and will be the topic of a separate study.

Future work will also include the application of the method on real-world cases, which will come with additional challenges. For example, we will have to consider the merging of neighboring glaciers when growing (a work already under way, Dusch,

25 2018). Importantly, the effect of uncertainties in the boundary conditions (in particular the glacier bed, its outlines and uncertainties in the climate forcing) will have to be quantified. Here again, the "surrogate world" framework will be useful by allowing data denial and data alteration experiments. To ensure the robust reconstruction of real-world glacier states additional changes and model developments are necessary, but our study is a first important step in this direction.

Code availability. The OGGM software together with initialization method are coded in the Python language and licensed under the

30 GPLV3 free software license. The latest version of the OGGM code is available on Github (https://github.com/OGGM/oggm), the documentation is hosted on ReadTheDocs (http://oggm.readthedocs.io), and the project webpage for communication and dissemination can be found at http://oggm.org. The OGGM version used in this study is v1.1. The code for the initialization module is available on Github (https://github.com/OGGM/initialization).

References

Auer, I., Böhm, R., Jurkovic, A., Lipa, W., Orlik, A., Potzmann, R., Schöner, W., Ungersböck, M., Matulla, C., Briffa, K., Jones, P., Efthymi-
adis, D., Brunetti, M., Nanni, T., Maugeri, M., Mercalli, L., Mestre, O., Moisselin, J.-M., Begert, M., Müller-Westermeier, G., Kveton, V.,
Bochnicek, O., Stastny, P., Lapin, M., Szalai, S., Szentimrey, T., Cegnar, T., Dolinar, M., Gajic-Capka, M., Zaninovic, K., Majstorovic, Z.,
5 and Nieplova, E.: HISTALP—historical instrumental climatological surface time series of the Greater Alpine Region, International Journal
of Climatology, 27, 17–46, https://doi.org/10.1002/joc.1377, https://rmets.onlinelibrary.wiley.com/doi/abs/10.1002/joc.1377, 2007.

Bamber, J., Westaway, R. M., Marzeion, B., and Wouters, B.: The land ice contribution to sea level during the satellite era, Environmental
Research Letters, https://doi.org/10.1088/1748-9326/aac2f0, 2018.

Cazenave, A. and et al.: Global sea-level budget 1993–present, Earth System Science Data, 10, 1551–1590, https://doi.org/10.5194/essd-10-
10 1551-2018, 2018.

Church, J., Clark, P., Cazenave, A., Gregory, J., Jevrejeva, S., Levermann, A., Merrifield, M., Milne, G., Nerem, R., Nunn, P., Payne,
A., Pfeffer, W., Stammer, D., and Unnikrishnan, A.: Sea Level Change, book section 13, p. 1137–1216, Cambridge University Press,
Cambridge, United Kingdom and New York, NY, USA, https://doi.org/10.1017/CBO9781107415324.026, www.climatechange2013.org,
2013.

15 Dusch, M.: OGGM feature development: "Allow individual glaciers to merge together", https://github.com/OGGM/oggm/pull/624, [Online;
accessed 28-May-2019], 2018.

Farinotti, D., Huss, M., Bauder, A., Funk, M., and Truffer, M.: A method to estimate the ice volume and ice-thickness distribution of alpine
glaciers, Journal of Glaciology, 55, 422–430, https://doi.org/10.3189/002214309788816759, 2009.

Farinotti, D., Brinkerhoff, D. J., Clarke, G. K. C., Fürst, J. J., Frey, H., Gantayat, P., Gillet-Chaulet, F., Girard, C., Huss, M., Leclercq,
20 P. W., Linsbauer, A., Machguth, H., Martin, C., Maussion, F., Morlighem, M., Mosbeux, C., Pandit, A., Portmann, A., Rabatel, A.,
Ramsankaran, R., Reerink, T. J., Sanchez, O., Stentoft, P. A., Singh Kumari, S., van Pelt, W. J. J., Anderson, B., Benham, T., Binder,
D., Dowdeswell, J. A., Fischer, A., Helfricht, K., Kutuzov, S., Lavrentiev, I., McNabb, R., Gudmundsson, G. H., Li, H., and Andreassen,
L. M.: How accurate are estimates of glacier ice thickness? Results from ITMIX, the Ice Thickness Models Intercomparison eXperiment,
The Cryosphere, 11, 949–970, https://doi.org/10.5194/tc-11-949-2017, https://www.the-cryosphere.net/11/949/2017/, 2017.

25 Farinotti, D., Huss, M., Fürst, J. J., Landmann, J., Machguth, H., Maussion, F., and Pandit, A.: A consensus estimate for the ice thickness
distribution of all glaciers on Earth, 12, 168 – 173, https://doi.org/10.1038/s41561-019-0300-3, 2019.

Gardner, A. S., Moholdt, G., Cogley, J. G., Wouters, B., Arendt, A. A., Wahr, J., Berthier, E., Hock, R., Pfeffer, W. T., Kaser, G., Ligtenberg,
S. R. M., Bolch, T., Sharp, M. J., Hagen, J. O., van den Broeke, M. R., and Paul, F.: A Reconciled Estimate of Glacier Contributions
to Sea Level Rise: 2003 to 2009, Science, 340, 852–857, https://doi.org/10.1126/science.1234532, http://science.sciencemag.org/content/
30 340/6134/852, 2013.

Giesen, R. H. and Oerlemans, J.: Calibration of a surface mass balance model for global-scale applications, The Cryosphere, 6, 1463–1481,
https://doi.org/10.5194/tc-6-1463-2012, https://www.the-cryosphere.net/6/1463/2012/, 2012.

Giesen, R. H. and Oerlemans, J.: Climate-model induced differences in the 21st century global and regional glacier contributions to sea-level
rise, Climate Dynamics, 41, 3283–3300, https://doi.org/10.1007/s00382-013-1743-7, https://doi.org/10.1007/s00382-013-1743-7, 2013.

35 Goelzer, H., Nowicki, S., Edwards, T., Beckley, M., Abe-Ouchi, A., Aschwanden, A., Calov, R., Gagliardini, O., Gillet-Chaulet, F., Golledge,
N. R., Gregory, J., Greve, R., Humbert, A., Huybrechts, P., Kennedy, J. H., Larour, E., Lipscomb, W. H., Le clec'h, S., Lee, V., Morlighem,
M., Pattyn, F., Payne, A. J., Rodehacke, C., Rückamp, M., Saito, F., Schlegel, N., Seroussi, H., Shepherd, A., Sun, S., van de Wal, R., and

Ziemen, F. A.: Design and results of the ice sheet model initialisation experiments initMIP-Greenland: an ISMIP6 intercomparison, The Cryosphere, 12, 1433–1460, https://doi.org/10.5194/tc-12-1433-2018, https://www.the-cryosphere.net/12/1433/2018/, 2018.

Goosse, H., Barriat, P.-Y., Dalaiden, Q., Klein, F., Marzeion, B., Maussion, F., Pelucchi, P., and Vlug, A.: Testing the consistency between changes in simulated climate and Alpine glacier length over the past millennium, Climate of the Past, 14, 1119–1133,
5   https://doi.org/10.5194/cp-14-1119-2018, https://www.clim-past.net/14/1119/2018/, 2018.

Gregory, J. M., White, N. J., Church, J. A., Bierkens, M. F. P., Box, J. E., van den Broeke, M. R., Cogley, J. G., Fettweis, X., Hanna, E., Huybrechts, P., Konikow, L. F., Leclercq, P. W., Marzeion, B., Oerlemans, J., Tamisiea, M. E., Wada, Y., Wake, L. M., and van de Wal, R. S. W.: Twentieth-Century Global-Mean Sea Level Rise: Is the Whole Greater than the Sum of the Parts?, Journal of Climate, 26, 4476–4499, https://doi.org/10.1175/JCLI-D-12-00319.1, https://doi.org/10.1175/JCLI-D-12-00319.1, 2013.

10   Harris, I. C., Jones, P. D., Osborn, T., and Lister, D.: Updated hight-resolution grids of montly climatic observations- the CRU TS3.10 Dataset, International Journal of Climatology, 34, 623–642, https://doi.org/10.1002/joc.3771, 2014.

Heimbach, P. and Bugnion, V.: Greenland ice-sheet volume sensitivity to basal, surface and initial conditions derived from an adjoint model, Annals of Glaciology, 50, 67–80, https://doi.org/10.3189/172756409789624256, 2009.

Huss, M. and Hock, R.: A new model for global glacier change and sea-level rise, Frontiers in Earth Science, 3, 54,
15   https://doi.org/10.3389/feart.2015.00054, https://www.frontiersin.org/article/10.3389/feart.2015.00054, 2015.

Jacob, T., Wahr, J., Pfeffer, W. T., and Swenson, S.: Recent contributions of glaciers and ice caps to sea level rise, Nature, 482, https://doi.org/https://doi.org/10.1038/nature10847, 2012.

Jarvis, A., Guevara, E., Reuter, H., and Nelson, A.: Hole-filled SRTM for the globe : version 4 : data grid, published by CGIAR-CSI on 19 August 2008., 2008.

20   Jóhannesson, T., Raymond, C. F., and Waddington, E. D.: A Simple Method for Determining the Response Time of Glaciers, in: Glacier Fluctuations and Climatic Change, edited by Oerlemans, J., pp. 343–352, Springer Netherlands, Dordrecht, 1989.

Kienholz, C., Rich, J. L., Arendt, A. A., and Hock, R.: A new method for deriving glacier centerlines applied to glaciers in Alaska and northwest Canada, The Cryosphere, 8, 503–519, https://doi.org/10.5194/tc-8-503-2014, https://www.the-cryosphere.net/8/503/2014/, 2014.

Leclercq, P. W., Oerlemans, J., and Cogley, J. G.: Estimating the Glacier Contribution to Sea-Level Rise for the Period 1800–2005, Surveys
25   in Geophysics, 32, 519, https://doi.org/10.1007/s10712-011-9121-7, https://doi.org/10.1007/s10712-011-9121-7, 2011.

Lee, V., Cornford, S. L., and Payne, A. J.: Initialization of an ice-sheet model for present-day Greenland, Annals of Glaciology, 56, 129–140, https://doi.org/10.3189/2015AoG70A121, 2015.

Marzeion, B., Jarosch, A. H., and Hofer, M.: Past and future sea-level change from the surface mass balance of glaciers, The Cryosphere, 6, 1295 – 1322, https://doi.org/10.5194/tc-6-1295-2012, 2012.

30   Marzeion, B., Cogley, J. G., Richter, K., and Parkes, D.: Attribution of global glacier mass loss to anthropogenic and natural causes, Science, 345, 919–921, https://doi.org/10.1126/science.1254702, http://science.sciencemag.org/content/345/6199/919, 2014.

Marzeion, B., Leclercq, P. W., Cogley, J. G., and Jarosch, A. H.: Brief Communication: Global reconstructions of glacier mass change during the 20th century are consistent, The Cryosphere, 9, 2399–2404, https://doi.org/10.5194/tc-9-2399-2015, 2015.

Marzeion, B., Kaser, G., Maussion, F., and Champollion, N.: Limited influence of climate change mitigation on short-term glacier mass loss,
35   Nature Climate Change, 8, 305–308, https://doi.org/10.1038/s41558-018-0093-1, 2018.

Maussion, F., Butenko, A., Champollion, N., Dusch, M., Eis, J., Fourteau, K., Gregor, P., Jarosch, A. H., Landmann, J., Oesterle, F., Recinos, B., Rothenpieler, T., Vlug, A., Wild, C. T., and Marzeion, B.: The Open Global Glacier Model (OGGM) v1.1, Geoscientific Model Development, 12, 909–931, https://doi.org/10.5194/gmd-12-909-2019, https://www.geosci-model-dev.net/12/909/2019/, 2019.

Mosbeux, C., Gillet-Chaulet, F., and Gagliardini, O.: Towards a better ice sheet model initialisation and basal knowledge using data assimilation, Geoscientific Model Development Discussions, pp. 1–24, https://doi.org/10.5194/gmd-2016-7, 2016.

Pfeffer, W. T., Arendt, A. A., Bliss, A., Bolch, T., Cogley, J. G., Gardner, A. S., Hagen, J. O., Hock, R., G., K., Kienholz, C., Miles, E. S., Moholdt, G., Mölg, N., Paul, F., Radić, V., Rastner, P., Raup, B. H., Rich, J., Sharp, M. J., and the Randolph Consortium: The Randolph

5   Glacier Inventory: a globally complete inventory of glaciers, Journal of Glaciology, 60, 537–551, https://doi.org/10.3189/2014JoG13J176, 2014.

Radić, V. and Hock, R.: Regionally differentiated contribution of mountain glaciers and ice caps to future sea-level rise, Nature Geoscience, 4, 91–94, https://doi.org/10.1038/ngeo1052, 2011.

Radić, V. and Hock, R.: Glaciers in the Earth's Hydrological Cycle: Assessments of Glacier Mass and Runoff Changes on Global and

10   Regional Scales, Surveys in Geophysics, 35, 813–837, https://doi.org/10.1007/s10712-013-9262-y, 2014.

Raup, B., Racoviteanu, A., Khalsa, S. J. S., Helm, C., Armstrong, R., and Arnaud, Y.: The GLIMS geospatial glacier database: A new tool for studying glacier change, Global and Planetary Change, 56, 101 – 110, https://doi.org/https://doi.org/10.1016/j.gloplacha.2006.07.018, 2007.

RGI Consortium: Randolph Glacier Inventory – A Dataset of Global Glacier Outlines: Version 6.0: Technical Report, Global Land Ice

15   Measurements from Space, Colorado, USA, https://doi.org/10.7265/N5-RGI-60, 2017.

Slangen, A. B. A., Adloff, F., Jevrejeva, S., Leclercq, P. W., Marzeion, B., Wada, Y., and Winkelmann, R.: A Review of Recent Updates of Sea-Level Projections at Global and Regional Scales, Surveys in Geophysics, 38, 385–406, https://doi.org/10.1007/s10712-016-9374-2, https://doi.org/10.1007/s10712-016-9374-2, 2017a.

Slangen, A. B. A., Meyssignac, B., Agosta, C., Champollion, N., Church, J. A., Fettweis, X., Ligtenberg, S. R. M., Marzeion, B., Melet, A.,

20   Palmer, M. D., Richter, K., Roberts, C. D., and Spada, G.: Evaluating Model Simulations of Twentieth-Century Sea Level Rise. Part I: Global Mean Sea Level Change, Journal of Climate, 30, 8539–8563, https://doi.org/10.1175/JCLI-D-17-0110.1, https://doi.org/10.1175/ JCLI-D-17-0110.1, 2017b.

van Pelt, W. J. J., Oerlemans, J., Reijmer, C. H., Pettersson, R., Pohjola, V. A., Isaksson, E., and Divine, D.: An iterative inverse method to estimate basal topography and initialize ice flow models, The Cryosphere, 7, 987–1006, https://doi.org/10.5194/tc-7-987-2013, https:

25   //www.the-cryosphere.net/7/987/2013/, 2013.

WGMS: Fluctuations of Glaciers Database, World Glacier Monitoring Service, Zurich, Switzerland, https://doi.org/10.5904/wgms-fog-2018-11, 2018.

Zekollari, H., Huss, M., and Farinotti, D.: Modelling the future evolution of glaciers in the European Alps under the EURO-CORDEX RCM ensemble, The Cryosphere, 13, 1125–1146, https://doi.org/10.5194/tc-13-1125-2019, https://www.the-cryosphere.net/13/1125/2019/,

30   2019.

Zemp, M., Frey, H., Gärtner-Roer, I., Nussbaumer, S. U., Hoelzle, M., Paul, F., Haeberli, W., Denzinger, F., Ahlstrøm, A. P., Anderson, B., and et al.: Historically unprecedented global glacier decline in the early 21st century, Journal of Glaciology, 61, 745–762, https://doi.org/10.3189/2015JoG15J017, 2015.